Journal of Mining and Environment (JME) Vol. 17, No. 3, 2026, 781-800

Shahrood University of Technology

Journal of Mining and Environment (JME)

Journal homepage: www.jme.shahroodut.ac.ir

Iranian Society of Mining Engineering (IRSME)

Applications of Machine Learning Models to Predict the Uniaxial Compressive Strength of Sandstone from Muzaffarabad - A Case Study

Barkat Ullah[1,2*], and Raja Khurram Mahmood Khan[3]

1. Research Center of Coastal and Urban Geotechnical Engineering, Zhejiang University, Zijingang, Hangzhou 310058, China
2. Computing Center for Geotechnical Engineering, Zhejiang University, Hangzhou, Zhejiang 310058, China
3. Department of Civil, Construction, Architectural, and Environmental Engineering, University of L'Aquila, L'Aquila 67100, Italy

Article Info

Received 2 July 2025

Received in Revised form 8 November 2025

Accepted 29 December 2025

Published online 29 December 2025

DOI: 10.22044/jme.2025.16419.3206

Keywords

K-fold cross-validation

Machine learning

Sandstone

Uniaxial compressive strength (UCS)

XGBoost

Abstract

Uniaxial compressive strength (UCS) is an essential feature for characterizing and classifying rock masses, forming a critical component of rock failure criteria with extensive applications in mining and geotechnical engineering. This study aims to evaluate the performance of different machine learning (ML) models in forecasting the UCS of sandstone obtained from the Murree and Kamlial formations in the Muzaffarabad area, northwestern Himalayas, Pakistan. The ML models—namely artificial neural network (ANN), adaptive neuro-fuzzy inference system (ANFIS), support vector regressor (SVR), random forest (RF), and extreme gradient boosting (XGBoost)—were developed to predict UCS (MPa) based on porosity (η), point load index (Is(50)), Schmidt hammer rebound value (Rn), and aggregate impact value (AIV) as input variables. A dataset containing 80 points was divided using a 70:30 split ratio for training and testing sets. K-fold cross-validation (with 5 to 10 folds) was employed to enhance the models' generalization ability. The performance of the models was evaluated using mean absolute error (MAE), mean square error (MSE), root mean square error (RMSE), and coefficient of determination (R^2). Results revealed that the XGBoost model outperformed the other models, achieving a high R^2 value of 0.99 and low error values for MAE (0.789), MSE (1.168), and RMSE (1.080). The overall accuracy of the models can be ranked as follows: XGBoost > RF > ANN > ANFIS > SVR. This study provides a benchmark for predicting the UCS of sandstones and similar rocks where complex geology complicates the collection of intact samples.

1. Introduction

Uniaxial compressive strength (UCS) is an essential feature in rock mass characterization, failure criteria [1,2], and has extensive applications in rock engineering projects [3]. Generally, UCS can be measured directly using standardized laboratory test methods, as documented in the recommendations of the International Society for Rock Mechanics (ISRM, 2007) and the American Society for Testing and Materials (ASTM, 1986) [4]. The direct method for determining UCS requires the collection of numerous standardized core samples from intact blocks following a careful procedure. However, this process of preparing samples for laboratory testing can be time-consuming and costly, especially the procedures needed to collect standardized core samples [4,5]. These expenses increase significantly for samples taken from highly fractured, weak, and weathered rocks (e.g., shale, mudstone, or sandstone) [6], or predominantly hard rocks (e.g., granite, granodiorite) [7], making the direct determination of UCS costly in terms of time and money [8]. Therefore, the use of indirect methods for UCS estimation is of great importance.

In recent years, researchers have emphasized alternative and indirect implementation of soft computing techniques [8], including ML approaches, to overcome problems in mining and

Corresponding author: barkat_ullah12@outlook.com (B. Ullah)

geotechnical engineering. These approaches are practical, rapid and effective in solving engineering problems, especially when there is an uncertain association between the dependent and independent variables [9,10]. The use of these approaches has proven to be economically more advantageous than the direct determination of UCS in the laboratory [8]. The traditional approach to creating prediction models include utilizing statistical methods such as simple and multiple regressions [1]. Such as Torabi et al., [11] proposed a new equation correlating the Schmidt hammer rebound number (n) with the UCS of a rock mass under specific geological conditions. These procedures are typically employed as individual methods for assessing rock strength characteristics, particularly when samples collection for laboratory tests is impossible. From a general point of view, the derived correlation only gives appropriate results in similar types of rocks [2]. Meanwhile, soft computing techniques, such as artificial neural networks (ANNs)[12], have demonstrated their capability to resolve complex difficulties in the fields of science, engineering, and even problems related to rock strength [13,14]. Singh et al., [15] recommended the application of neural networks to predict UCS, tensile strength and axial point load strength simultaneously from the mineralogical composition, area weighting, form factor, aspect ratio, grain size, and orientation of foliation planes of four kinds of schistose rocks. Fattahi & Babanouri, [16] introduced a novel methodology that integrates support vector regression (SVR) with a cultural algorithm (CA) to predict the tensile strength of rocks based on their physical characteristics. Based on the results of index tests of sedimentary rocks, Jalali et al., [17] developed a fuzzy interface system (FIS), ANN and ANFIS models to predict UCS. An ANN model was proposed by Abdi et al., [18] to predict UCS and Young's modulus (E) from sedimentary rock data. Fattahi[19] presented a novel intelligence method, relevance vector regression (RVR), enhanced by the cuckoo search (CS) and harmony search (HS) algorithms, to predict UCS of weak rocks (UCSWR). Shahani et al., [20] developed XGBoost model to predict E and UCS of intact sedimentary rocks. Armaghani et al., [21] presented ANFIS as a predicting model for E and UCS for granite in Malaysia. Sharma et al., [4] employed ANFIS as a capability model to predict UCS of different rocks and later compared the performance of the proposed model with ANN and multi regression (MR) models. Armaghani et al., [22] proposed the application of several modeling techniques, including linear multiple regression (LMR), non-linear multi regression (NLMR), ANN and hybrid imperialism competitive algorithm (ICA-ANN) for UCS prediction. A study by Fang et al., [13] used ANN, artificial bee colonies (ABC-ANN), and genetic programming (GP) to estimate the UCS of granite rock. Two different models, such as MR and ANN, were used by Zorlu et al., [23] to study the relationship between petrographic properties and strength of sandstones.

Recently, it has become more common for ML-based methods to be adopted for predicitng the UCS of rocks due to their simplicity, hustle, and rationality. Thus, the researchers attempt to develop some cutting-edge predicting models for the accurate estimation of UCS. Similarly, Wan et al., [24] used linear regression (LR), SVR, XGBoost and ANN to predict the UCS of concrete based on its curing age and mixture composition. A beetle antennae search (BAS) algorithm based RF model has been developed by Zhang et al., [25] to predict the UCS of lightweight self-compacting concrete (LWSCC). Mai et al., [26] anticipated an approach, namely RF, for predicting the UCS of concrete using ground granulated blast furnace slag (GGBFS). Matin et al., [27] used the RF model to choose variables within several rock properties and indexes to construct an effective predictive model for UCS and E. A regression model based on XGBoost is established by Nguyen-Sy et al., [28] for predicting the UCS of concrete based on its composition and age. Based on SVR, Negara et al., [29] proposed a data-driven universal model for UCS prediction. Sun et al., [30] proposed a B-based modified evolved SVR to accurately and effectively predict the pervious concrete's permeability coefficient (PC) and UCS (MPa). To forecast the UCS of stabilized pond ashes with lime and lime sludge, Suthar, [10] evaluated five different prediction modeling approaches. A RF model was proposed by Wang et al., [31] for accurately predicting a rock's UCS based on simple index tests. Abdi et al., [32] predicted the UCS and E of sandstones from petrographic characteristics using an ANN and multiple regression. Their results demonstrated that ANN performed well in prediction with R^2 value of 0.92. Köken [33] employed soft computing techniques, including classification and regression trees (CART), multiple adaptive regression splines (MARS), ANFIS, ANN, and gene expression programming (GEP), to forecast the UCS of pyroclastic rocks. The results revealed that the coefficient of determination (R^2) for the models ranges from 0.82 to 0.88. Furthermore, Jamshidi [34] conducted a

comparative study point load index test procedures in predicting the uniaxial compressive strength of sandstones. The point load index test is performed in four procedures: axial, diametrical, block, and irregular lump tests demonstrating that the axial has high accuracy in predicting UCS. Although, these studies have achieved fruitful insights into UCS prediction of rocks and rock-like materials, still, a wide range of cutting-edge ML models remains essential, particularly in areas where sample collection is challenging as a result of complex geological layouts (see Figure1) and limited access. Therefore, further research on utilising soft-computing methods is immensely needed to overcome the stated limitations in areas where the sampling collection is challenging for laboratory tests. Table 1 lists the results of some previous studies using soft computing methods to estimate UCS.

Table 1. Previous research using soft computing methods to estimate mechanical properties.

S. No	Material	Models	Outputs	Performance (R^2)	References
1	Granite	XGBoost-FA	UCS (MPa) E(GPa)	0.98 0.97	[35]
2	Soft sedimentary rocks	ANFIS	UCS (MPa) E(GPa)	0.95 0.91	[36]
3	Granitic Rocks	ANFIS	UCS (MPa)	0.95	[22]
4	Granite	GP	UCS (MPa)	0.84	[13]
5	Sedimentry rocks	SR	UCS (MPa)	0.97	[37]
6	Sandstone	ICA-ANN	UCS (MPa)	0.94	[38]
7	Weak rocks	RVR-HS	UCS (MPa)	0.99	[19]
8	Intact rocks	ANFIS-GA, ANFIS-PSO	UCS (MPa)	0.97	[39]
9	Concrete	SVR, XGBoost	UCS (MPa)	0.93	[24]
10	Sandstones	ANN	UCS (MPa) E (GPa)	0.92 0.87	[32]
11	Carbonate Aggregates	ANN	UCS (MPa)	0.92	[40]
12	Concrete	BAS-RF	UCS (MPa)	0.97	[25]

FA – Firefly algorithm; XGBoost – Extreme Gradient Boosting; ANFIS – Adaptive Neuro-Fuzzy Inference System; GP – Genetic Programming; PSO – Particle Swarm Optimization; SR – Simple Regression; ICA – Imperialist Competitive Algorithm; ANN – Artificial Neural Network; SVR – Support Vector Regression; RVR – Relevance Vector Regression; HS – Harmony Search; BAS – Beetle Antennae Search; RF – Random Forest

2. Contribution of the study

This study was conducted on sandstone obtained from outcrops of the Murree and Kamlial formations of Muzaffarabad. Previously, Muzaffarabad sandstone was the main focus of many researchers; however, their work was generally limited to stratigraphy, geology, petrography, and structure, and did not meet the practical criteria of rock engineering project design. To date, predicting the mechanical properties of Muzaffarabad sandstone using machine learning (ML) techniques has been largely overlooked, highlighting the need to explore this aspect. Therefore, this is the first attempt to apply and compare this specific suite of ML models for UCS prediction in this particular geological setting. Consequently, it is crucial to develop ML-based prediction models by establishing the proper relationship between the physical and mechanical parameters of sandstone. To achieve this, this study employs ANN, ANFIS, SVR, RF, and XGBoost models to predict UCS using η, $Is_{(50)}$, Rn, and AIV as input variables. The developed models are then evaluated based on performance indices, including MAE, MSE, RMSE, and R^2.

3. Geological layout of the study area

The samples used in this study include sandstone collected from different outcrops of the Murree and Kamlial formations in the Muzaffarabad region of the northwestern Himalayas in Pakistan. The local construction industry uses the region's sandstone as a building stone and aggregate material. The study area is located in the tectonically active region of the northwestern Himalayas. The active fault in the area, known as the Kashmir boundary thrust (KBT), has caused significant shearing, weathering, and internal fracturing of the rocks [41]. The KBT resulted from a devastating earthquake in the region in 2005. The Murree formation has a thrust lower contact with the upper Abbottabad formation, which is associated with the KBT. The active fault zone nearby renders the Abbottabad formation highly fractured and jointed [41]. Moreover, the area lies within the core of the Hazara-Kashmir syntaxis in the sub-Himalayas. Himalayan orogeny is the world's youngest active continental-to-continental collision. Figure 1 shows the detailed geological distribution of the Murree and Kamlial formations. Due to fractures

and joints, collecting block samples becomes very challenging. Therefore, establishing reliable prediction models for strength is essential to guide safe slope design, ensure foundation stability, and reduce construction hazards in this seismically susceptible region of the northwestern Himalayas. To achieve this, 11 locations (as shown in Figure 1) were selected for sampling, and a dataset containing 80 points was compiled to account for sample homogeneity.

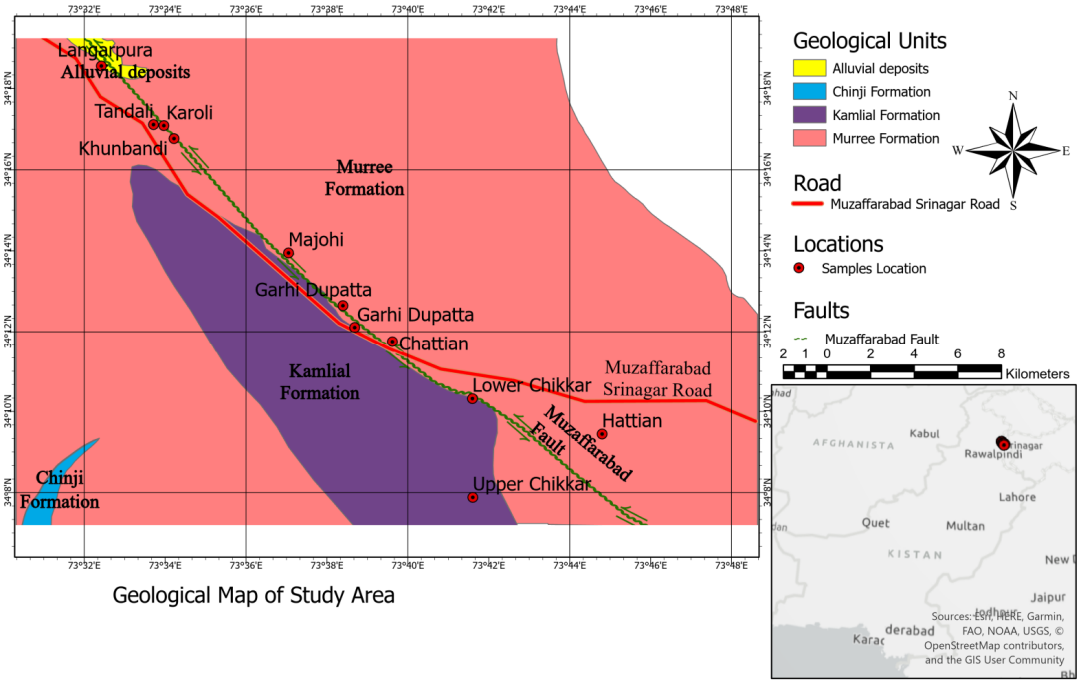

Geological Map of Study Area

Figure .1 Geological setting of the study area.

4. Dataset construction

4.1. Data collection

This study uses the database prepared by a series of laboratory tests on sandstone samples collected from different blocks. The samples obtained from the study area were taken to the laboratory to conduct physical and mechanical tests. The tests were conducted in Azad Jammu and Kashmir university (AJKU), Muzaffar Abad, Pakistan. The tests were performed according to the standards recommended by ASTM. The dataset includes the following tests: η (m/v), $Is_{(50)}$ (MPa), R_n, AIV, and UCS (MPa). The details of the tests are listed in the following sub-sections.

4.1.1. Porosity

Effective porosity was determined following the standard procedure outlined in ASTM D 7063. Core samples were first oven-dried to a constant mass to establish their dry weight. Subsequently, the samples were placed in a perforated basket and fully submerged in a water tank for a 48-hour saturation period. After immersion, the saturated weight was measured in two ways: first, as the suspended weight in water, and then as the saturated surface-dry weight after carefully blotting the specimens with an absorbent cloth to remove any surface water film. Porosity can then be calculated using the following expressions.

$$\text{Specific gravity} = \frac{\text{Dry weight}}{\text{Saturated surface dry weight}} - \text{Suspended load}$$

$$\text{Apparent specific gravity} = \frac{\text{Saturated surface dry weight}}{\text{Saturated surface dry weight}} - \text{Suspended load}$$

$$\text{Effective porosity} = \frac{\text{Apparent specific gravity}}{\text{Specific gravity}} - \text{Apparent specific gravity} \times 100$$

4.1.2. Point load index ($Is_{(50)}$)

The point load test is widely used for estimating the strength of rock materials. Its primary value lies in providing a quick and inexpensive means to determine the $Is_{(50)}$, which can be correlated to the UCS for applications like rock mass classification and slope design. A key advantage of the test is its portability and minimal sample preparation requirements; it can be performed in the field on irregular rock lumps or core samples, as outlined in ASTM D-5731 (ASTM, 1985)[42]. In the axial test variant, a rock specimen of limited length is placed between two conical, hardened steel plates. A compressive load is applied through a hydraulic jack until the sample fails. The failure occurs due to tensile cracking induced by the concentrated point loads, not by direct compression. The failure load is recorded and used to calculate the point load strength index using the following formula.

$$I_s = \frac{P \times 1000}{{D_e}^2} \quad (1)$$

Where P (kN) is the failure load, D_e (mm) is equavelent diameter which can be calculated as follows.

$$D_e = \sqrt{\frac{4A}{\pi}} \quad (2)$$

Where, A (mm^2) represents cross-sectional area. The corrected value of $I_{s(50)}$ can be achieved as follows:

$$I_{s(50)} = I_s \times \left(\frac{D_e}{50}\right)^{0.45} \quad (3)$$

4.1.3. Aggregate impact value

The aggregate impact test was conducted using an impact testing machine, a tamping rod, sieves with apertures of 10 mm and 2.36 mm, and a precision balance. A 1 kg oven-dried sample, retained on the 10 mm sieve, was placed into the machine's cylindrical measure and compacted in three layers, with each layer receiving 25 blows from the tamping rod. The sample was then subjected to 15 hammer blows from the impact machine. The resulting material was sieved on the 2.36 mm sieve, and the weight of the fraction passing through (W2) was recorded. The AIV, expressed as a percentage, was calculated from the original sample weight (W1) using the formula:

$$\text{AIV} = (\text{W2} / \text{W1}) \times 100\% \quad (4)$$

4.1.4. Schmidt hammer rebound value (Rn)

Schmidt hammer testing was conducted according to ASTM D-5873-14. The instrument was held firmly against the sample surface with its plunger perpendicular to the test point. The hammer was then activated, and the rebound value was recorded from the scale. Rebound numbers were documented for each sample in both dry and saturated conditions.

4.1.5. Uniaxial compressive strength (UCS)

The UCS of the rock specimens was determined following the ASTM D2938 standard. Core samples were first cut to appropriate dimensions, and their end surfaces were ground flat and parallel to ensure uniform load distribution. Specimens meeting dimensional and surface smoothness criteria were then axially loaded in an automatic system compression frame equipped with a UCS device (45-C7022/S). A constant loading rate of 1 MPa/sec was applied until specimen failure. The compressive strength was calculated as the maximum sustained load per unit area.

4.2. Statistical description of the dataset

The statistical description, i.e., mean, standard deviation, minimum, and maximum values of each input and output parameter, is listed in Table 2. The correlation of UCS (MPa) with the input parameters is visualized by a distribution plot, as shown in Figure 2. It is worth mentioning that among all the input parameters considered for predicting the UCS (MPa) of the sandstone, $Is_{(50)}$ (MPa) and Rn exhibit a slightly stronger correlation with UCS (MPa). Conversely, η (m/v) and AIV demonstrate weak correlations with UCS (MPa).

As shown in Figure 3, a correlation index adjacent to 1 designates a strong positive relationship with the output parameter. In contrast, a correlation index -1 corresponds to a perfect negative correlation between two features moving in opposite directions. Two uncorrelated or weakly correlated features have a correlation value near zero.

Table 2. The statistical description of the dataset.

	Porosity (η)	Point Load Index ($Is_{(50)}$) (MPa)	Schmidt Rebound (Rn)	Aggregate Impact Value (AIV)	Uniaxial Compressive Strength (UCS) (MPa)
Mean	0.8347	1.0145	41.6888	21.6483	61.8221
Standard deviation	0.2074	0.9938	4.9371	7.9452	17.6668
Minimum	0.3400	0.1000	31.0000	7.1000	37.5000
Maximum	1.2400	4.3000	53.0000	37.5000	107.1400

Figure 2. Correlation and statistical distribution between input and output parameters

Figure 3. Heatmap correlation between input and output parameters

5. Machine learning models

In this study, the dataset was grouped into training (70%) and testing (30%) sets to avoid the problem of overfitting may occur when ML models are trained on the whole dataset [28]. Further, five ML models, i.e., ANN, ANFIS, SVM, RF, and XGBoost, were trained to accurately predict the UCS of sandstone. The stepwise procedure is displayed in a flow chart shown in Figure.4.

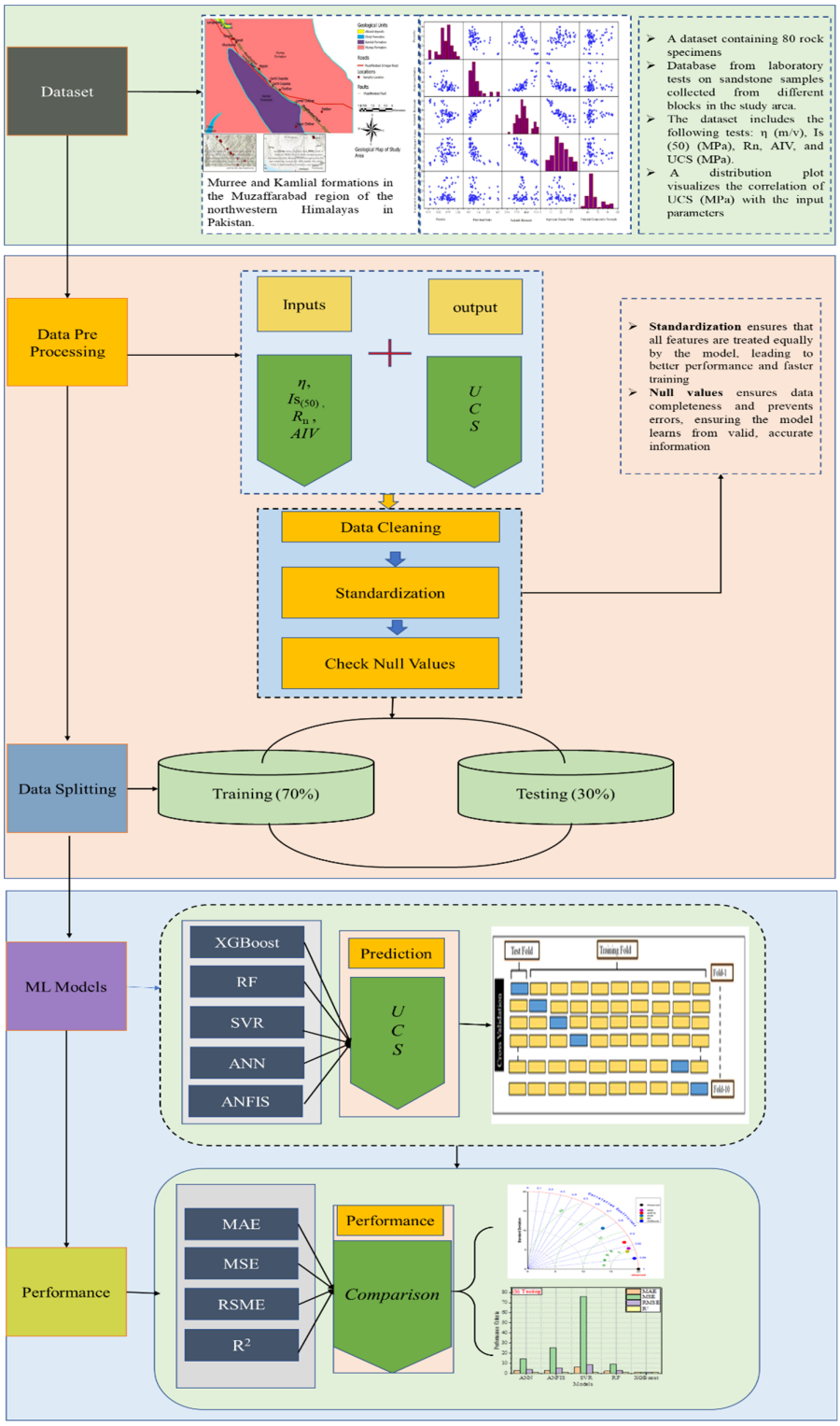

Figure 4. Flow chart of the study

5.1. Artificial neural network

ANN is composed of three main components: a learning algorithm, a transfer function, and a signal processing element called neurons. These neurons are considered highly interconnected processing elements that work together to achieve the goal [43]. A typical neural network contains three layers: an input layer, a hidden layer, and an output layer, as presented in Figure 5. The layers are connected by auxiliary functions called weights and biases, and the model's performance depends on the tuning of these weights and biases [44]. To achieve the desired design objectives, a learning algorithm modifies the synaptic weights of the network to facilitate the learning process [5]. The ANN model was trained using a feedforward back-propagation neural network (FFBP) because of its simplicity and applicability. In networks with multiple layers, learning algorithms such as back-propagation (BP) are commonly employed [18].

Furthermore, a Levenberg-Marquardt algorithm was used, which is the fastest method for training moderately sized feed-forward neural networks. The TRAINLM and LEARNGDM functions were utilized for training and adaptation, respectively. Similarly, a type-3 fuzzy inference system, consisting of five layers and producing a linear or constant output, was employed in this study. Different numbers of epochs were tested during training of the ANN, but the best fit was obtained at 6 epochs. Moreover, the number of neurons (nine neurons) was selected according to Equation 5, where N describes the number of inputs.

$$N_n \leq 2 \times N + 1 \quad (5)$$

5.2. Adaptive neuro-fuzzy inference system

The ANFIS is an ML approach that consolidates the FIS concept into an ANN and has been widely used in geotechnical engineering [45]. The ANFIS is advantageous for use when classical approaches are unsuccessful or highly complex in achieving the objective [46]. For the first-order Sugeno fuzzy model, the typical fuzzy reasoning mechanism of the ANFIS model with two fuzzy if-then rules is expressed as [43,47].

Rule-1: IF x is A_1 and y is B_1, THEN $f_1 = r_1x + s_1y + t_1$

Rule-2: IF x is A_2 and y is B_2, THEN $f_2 = r_2x + s_2y + t_2$.

To estimate UCS using some rock properties, a standard ANFIS model was developed employing the same datasets. The ANFIS was created by adopting the Sugeno model and a triangular membership function. Different numbers of epochs were tested during training, but the best fit was obtained at 200 epochs. The minimum validation error was used as the stopping criterion to prevent overfitting. The architecture of the ANFIS is depicted in Figure 6. The structure of the ANFIS contains five distinct layers.

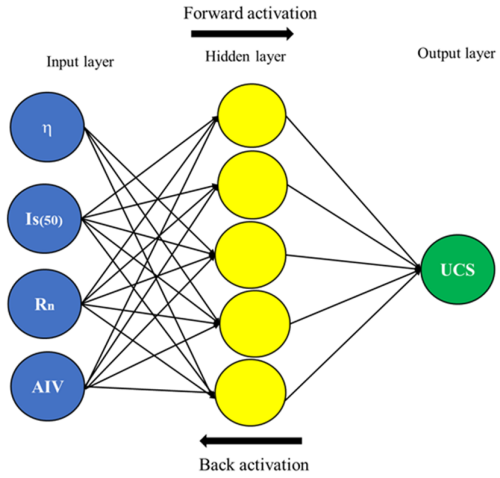

Figure 5. The architecture of artificial neural network

5.3. Support vector machine

The SVM has fewer regulating parameters, less overfitting problems, and an expanded convergence range to the global optimum, making it widely used in regression analysis, pattern recognition, and classification of large-scale nonlinear data to overcome the shortcomings of traditional ANNs [1]. By introducing kernel and Vapnik's -insensitive loss functions, SVM constructs prediction functions on a high-dimensional feature space [29]. For a dataset T = $\{(x_1, y_2), (x_2, y_2)\ldots(x_n, y_n)\}$ where $x_i \in R^n$ are the inputs and $y_i \in R^n$ are the outputs. To separate non-linear inputs into hyperplanes, SVM uses kernel functions to map them into high-dimensional feature space and using linear regression, these inputs can be related to outputs [48]. The SVM examined many kernel functions, including linear functions, polynomials, sigmoid functions, Gaussian functions, radial functions, and exponential radial functions [1]. The support vector regressor was used by importing SVM from Scikit-learn package in Python to obtain the regression results. Different kernel functions were checked and the linear function was selected as best for good performance. The training performance of the

model has not been affected by kernel parameters. Therefore, the default kernel parameters were used.

5.4. Random forest (RF)

The RF algorithm combines bootstrap and aggregation concepts to establish a large number of classification or regression trees (CARTs) [49]. The fundamental principles of RF involve constructing a forest by randomly selecting many decision trees, with the requirement that each decision tree in the RF is uncorrelated [27]. For regression analyses, samples of the input variables are used to fit the output variables. The data are divided into several points for each input variable, and the sum of squared errors (SSE) between the predicted and actual values is calculated at each division point. The minimum SSE value for each node is then determined. It is also possible to assess the impact of variables by arranging all their values and comparing their predictive accuracy among out-of-bag samples (a subset of observations not used during training, known as the "out-of-bag" dataset) [49]. The bootstrap-aggregated decision tree reduces overfitting by combining the results of many decision trees, thereby enhancing the model's ability to generalize [31]. It has been demonstrated that overfitting can be mitigated by using m trees.

The RF model was trained by using sklearn.ensemble Python package. From sklearn.ensemble, the RF regressor was imported. The number of estimators used is 50, and randomized data (random_state = 42) splitting was used. The random forest model was perfectly trained by the default parameters setting and a good performance result was obtained. Therefore, the hyperparameter tunning for RF was avoided.

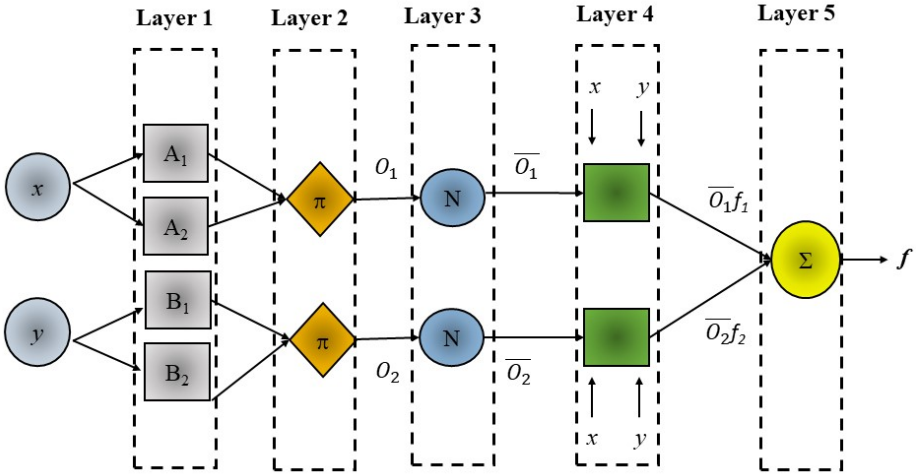

Figure 6. The general architecture of ANFIS model

5.5. Extreme gradient boosting (XGBoost)

As a successful tree-based ensemble learning algorithm, XGBoost is considered to be a useful asset among data science researchers. Based on gradient boosting architecture [50], the objective function of XGBoost is computed as follows in Equation (6):

$$Obj^{(t)} \approx \sum_{i=1}^{n}\left[L(y_i,\hat{y}_i) + g_i f_{i_{(xi)}} + \frac{1}{2}h_i f_i^2(x_i)\right] + \Omega(f_i), \quad (6)$$

where, the first part represents the training loss of the model, including both the logistic and squared loss, while the second part represents total tree complexity. The kth complexity of the tree can be calculated using $\Omega(f) = \gamma Q_t + \frac{1}{2}\varepsilon||M||^2$, where γ denotes the complexity parameter, Q_t denotes the number of leaf nodes, ε denotes constant coefficient, and $||M||^2$ denotes the l2-norm of the leaf weight.

Furthermore, the primary goal function, which follows Taylor expansion can be determined as follows in Equation (7):

$$= \sum_{i=1}^{n}\left[g_i m_i(x_i) + \frac{1}{2}h_i m_q^2(x_i)\right] + \gamma Q_t + \frac{1}{2}\sum_{j=1}^{Q_t} m_j^2 \quad (7)$$

$$= \sum_{i=1}^{Q_t}\left[\left(\sum_{i=I_j} g_i\right)M_j\frac{1}{2}\left(\sum_{i=I_j} h_i + \varepsilon\right)m_j^2\right] + \gamma Q_t \quad (8)$$

$$= \sum_{i=1}^{Q_t}\left[G_i m_i + \frac{1}{2}(H_j+\lambda)m_j^2\right] + \gamma Q_t\,, \quad (9)$$

In which, $g_i = \theta_{\hat{y}^{(t-1)}} L\left(y_i, \hat{y}^{(t-1)}\right), h_i = \theta^2_{\hat{y}^{(t-1)}} L\left(y_i, \hat{y}^{(t-1)}\right)$, I is the sample group of each leaf, $I_j = \{i \backslash q x_i = j\}$, $G_j = \sum_{i=I_j} g_i$, $H_j = \sum_{i=I_j} h_j$

XGBoost employs a second-order Taylor expansion as its objective function, rather than conventional gradient boosting. As indicated in the above equations (7–9), XGBoost accelerates the convergence process because, during model development, the first and second derivatives are calculated in parallel. Additionally, XGBoost includes a regularization term that smooths the responses of each decision tree, preventing overfitting. The model was trained using the reg:squared-error objective function. Considering a standard XGBoost model with default parameters in the XGBoost package—namely, M = 100 estimators, a learning rate of 0.1, and regularization parameters λ = 1 and γ = 0—the best R-squared values for both training and testing sets were obtained. In both sets, the optimal R-squared values were achieved with the default parameters of the XGBoost package. The constructed XGBoost model used M = 100 estimators, a learning rate (η) of 0.1, and regularization parameters λ = 1 and γ = 0.

6. Performance evaluation and cross-validation

6.1. Performance indicators

To evaluate the accuracy of the models, different indicators were adopted, including mean absolute error (MAE), mean square error (MSE) and root mean square error (RMSE) [51] and coefficient of determination (R^2) [52]. R^2 determine the correlation between the predicted and actual values in the range [0, 1]. The model exhibits high-performance accuracy when R^2 approaches 1. Meanwhile, low MAE, MSE, and RMSE indicate better ML model accuracy. Using the following equations, the values of performance indicators were obtained [53].

$$MAE = \frac{1}{n}\sum_{i=1}^{n}|U_m - U_p|\,, \quad (10)$$

$$MSE = \frac{1}{n}\sum_{i=1}^{n}(U_m - U_p)^2, \quad (11)$$

$$RMSE = \sqrt{\frac{1}{n}\sum_{i=1}^{n}(U_m - U_p)^2}\,, \quad (12)$$

$$R^2 = \frac{\left[\sum_{i=1}^{n}(U_m-\hat{U}_m)(U_p-\hat{U}_p)\right]^2}{\left[\sum_{i=1}^{n}(U_m-\hat{U}_m)^2(U_m-\hat{U}_m)^2\right]}, \quad (13)$$

where n is the number of the observations, U_m and U_p are measured and predicted values, respectively. $\hat{U}_m$ and $\hat{U}_p$ represents the mean measured values of actual and predicted UCS.

6.2. K-fold cross-validation

This study implemented *K*-fold cross-validation to minimize bias associated with the random partitioning of training and validation data [54], where *K* represents the number of folds. By partitioning the dataset into different subsets and evaluating their performance on each subgroup, cross-validation can determine the validity and accuracy of machine learning models [25]. In this way, reliability and generalization can be improved. In this study, the *5* to *10*-folds cross-validations (CV) is applied (see Figure 2) in the training sets, which splits the datasets into *5* to *10* mutually exclusive subsets (or folds) that are resembled with a study [55].

7. Results and discussion

7.1. Prediction performance of ML models

The prediction result of training sets and testing sets is listed in Table 3. Satisfactory results of the model's prediction are unveiled in terms of the statistical performance criteria in testing dataset. Results indicated that all the models are well fit to predict the UCS of sandstone. However, SVR somehow shows poor performance both in training and testing. The relatively low prediction errors obtained by these models in training compared to testing suggest that these models exhibit relatively good generalization ability compared to prediction. The performance indicators, including MAE, MSE, RMSE and R^2 values for ANN models in testing data are 2.77, 14.46, 3.803 and 0.96, respectively. The MAE, MSE, RMSE and R^2 values of ANFIS for testing set are 2.968, 25.49, 5.049 and 0.93 indicating the model was trained very well but dramatic changes are noticed in the testing. The low prediction of the SVR model with linear function in testing can be evident from high MAE, MSE and RMSE and low R^2 values 6.29, 76.01, 8.718 and 0.79, respectively. The performance of RF indicates that model performed well and obtained accurate results. The values of MAE, MSE, RMSE and R^2 for testing of RF are 2.266, 9.238, 3.033 and 0.97, respectively. The XGBoost gives the values of MAE, MSE, RMSE and R^2 of 0.789, 1.167, 1.080 and 0.99 for test dataset. Conclusively, the findings revealed that the XGBoost model had exceptional and consistent performance with the greatest R^2 value and the

lowest error metrics compared to all other models. The ANFIS model demonstrated signs of overfitting, seen in its outstanding performance on the training data, which significantly declined on the testing data suggesting it may have learned the noise in the training set rather than the underlying pattern. This indicates that although ANFIS could accurately model the training data, its ability to generalize to unseen data was rather constrained. The RF model demonstrated strong performance, albeit marginally surpassed by XGBoost.

Table 3. Performance of models on training and testing dataset.

Models	Training				Testing			
	MAE	MSE	RMSE	R^2	MAE	MSE	RMSE	R^2
XGBoost	0.741	0.958	0.978	0.99	0.789	1.167	1.080	0.99
RF	1.465	3.951	1.987	0.98	2.266	9.238	3.033	0.97
ANN	2.58	12.23	3.497	0.95	2.77	14.46	3.803	0.96
ANFIS	0.2689	0.4820	0.6943	0.99	2.968	25.49	5.049	0.93
SVR	5.769	62.98	7.934	0.77	6.29	76.01	8.718	0.79

Measured and predicted UCS (MPa) values by the models in the training and testing datasets are visualized in Figure 7 and Figure 8. The prediction performance is depicted by an error curve shown on the horizontal axis, indicating the prediction accuracy for both testing and training. As shown in Figure 7, all models demonstrate good training accuracy except for SVR. Models with high training accuracy exhibit lower error and less deviation among data points. Additionally, Figure 8 presents a comparison of measured and predicted UCS (MPa) values for the test dataset using five distinct predictive models. In each plot, the red circles represent the measured UCS (MPa) values, the black dots denote the predicted values, and the cyan bars illustrate the prediction errors. All models effectively capture the overall trend of the measured UCS (MPa) values; however, differences in prediction accuracy and error magnitude are evident among them. The ensemble models, specifically RF and XGBoost, display enhanced

7.2. Models comparison and discussions

This part of the study compared the prediction performance of models. Table 2 and Figure 11a & b summarize the performance indicators for each model. The models were assessed utilizing four statistical performance metrics such as MAE, MSE, RMSE, and the R^2. SVR demonstrates highest MSE and RMSE values in both datasets, signifying inferior prediction performance and larger divergence from the observed UCS values. Conversely, the ensemble learning models, specifically RF and XGBoost, exhibit the lowest error metrics and greatest R^2 values, indicating their enhanced accuracy and generalization capabilities. The reliable performance of these ensemble approaches on both training and testing datasets illustrates their robustness and appropriateness for modeling the nonlinear interactions intrinsic to rock strength prediction. The results correspond closely with the patterns depicted in Figure 8, wherein RF and XGBoost exhibited the highest concordance between the measured and anticipated UCS values, thereby reinforcing their reliability for geotechnical data modeling.predictive accuracy with reduced and more uniform error distributions, underscoring their effectiveness in modeling the complex, nonlinear interactions present in the geotechnical dataset. Based on these observations, the models can be successfully employed to predict the UCS (MPa) of sandstone from the Murree and Kamlial formations in the Muzaffarabad region.

Furthermore, the strength of a linear relationship between the actual and predicted UCS values in training and testing is justified by measuring the R^2 on a scatter plot, as depicted in Figures. 9 and Figure 10. The scattered points show the prediction values of the UCS by different models, while the straight line indicates the best performance result. The high R^2 in the training set (0.99) and testing set (0.99) demonstrates the high predictive capability of the XGBoost model followed by RF.

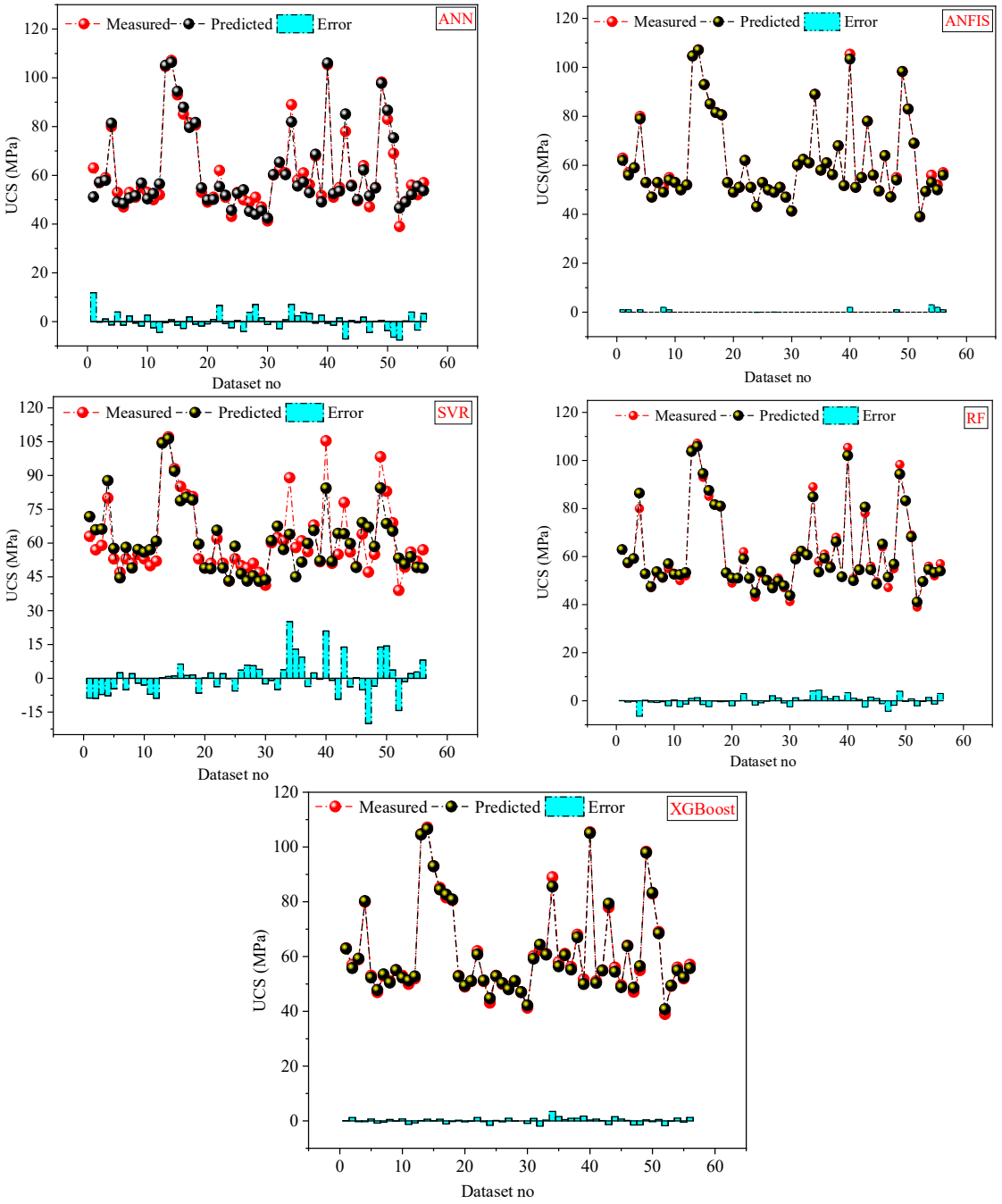

Figure 7. Comparison of actual and predicted values of models on training dataset

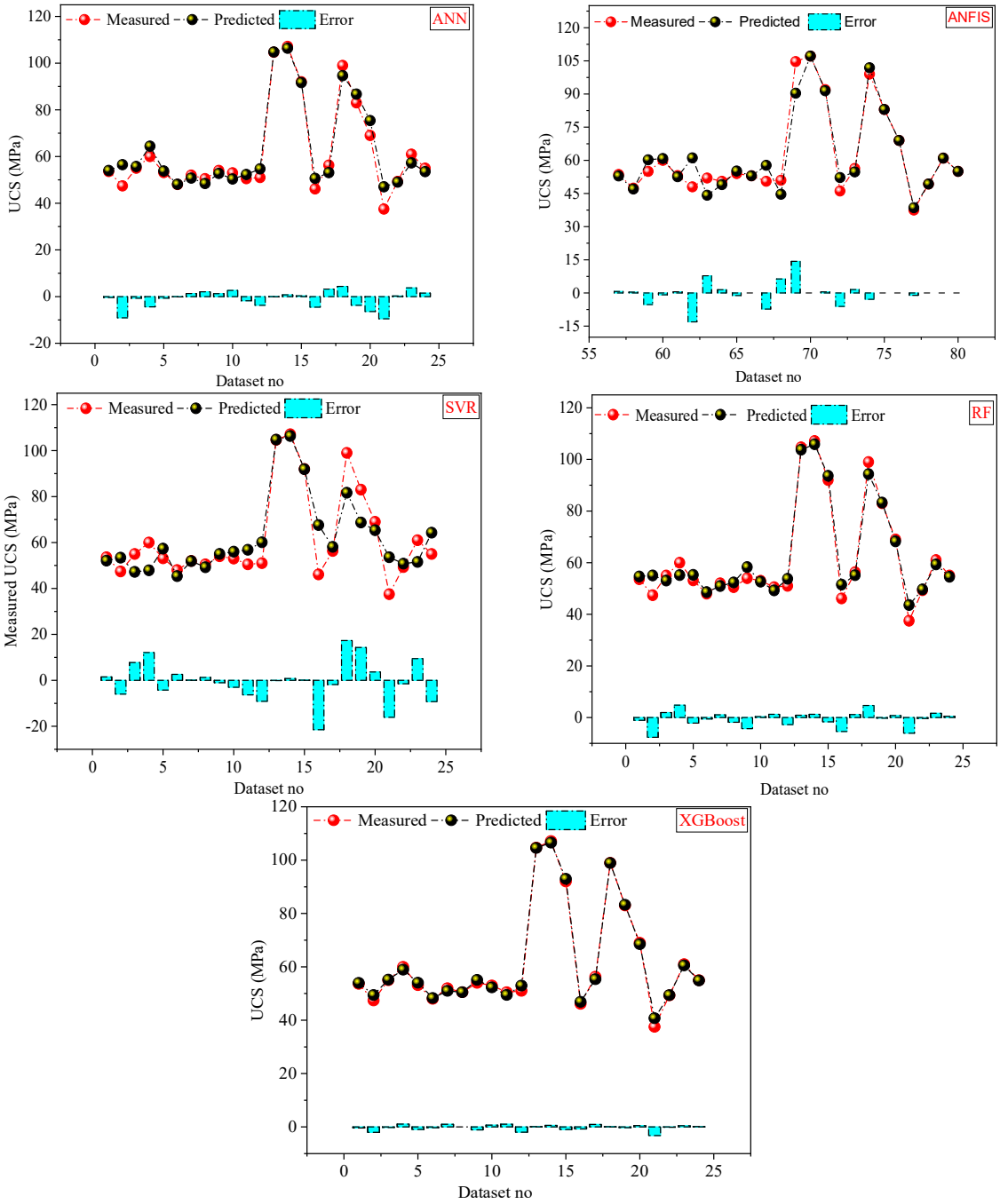

Figure 8. Test dataset comparison between actual and predicted values.

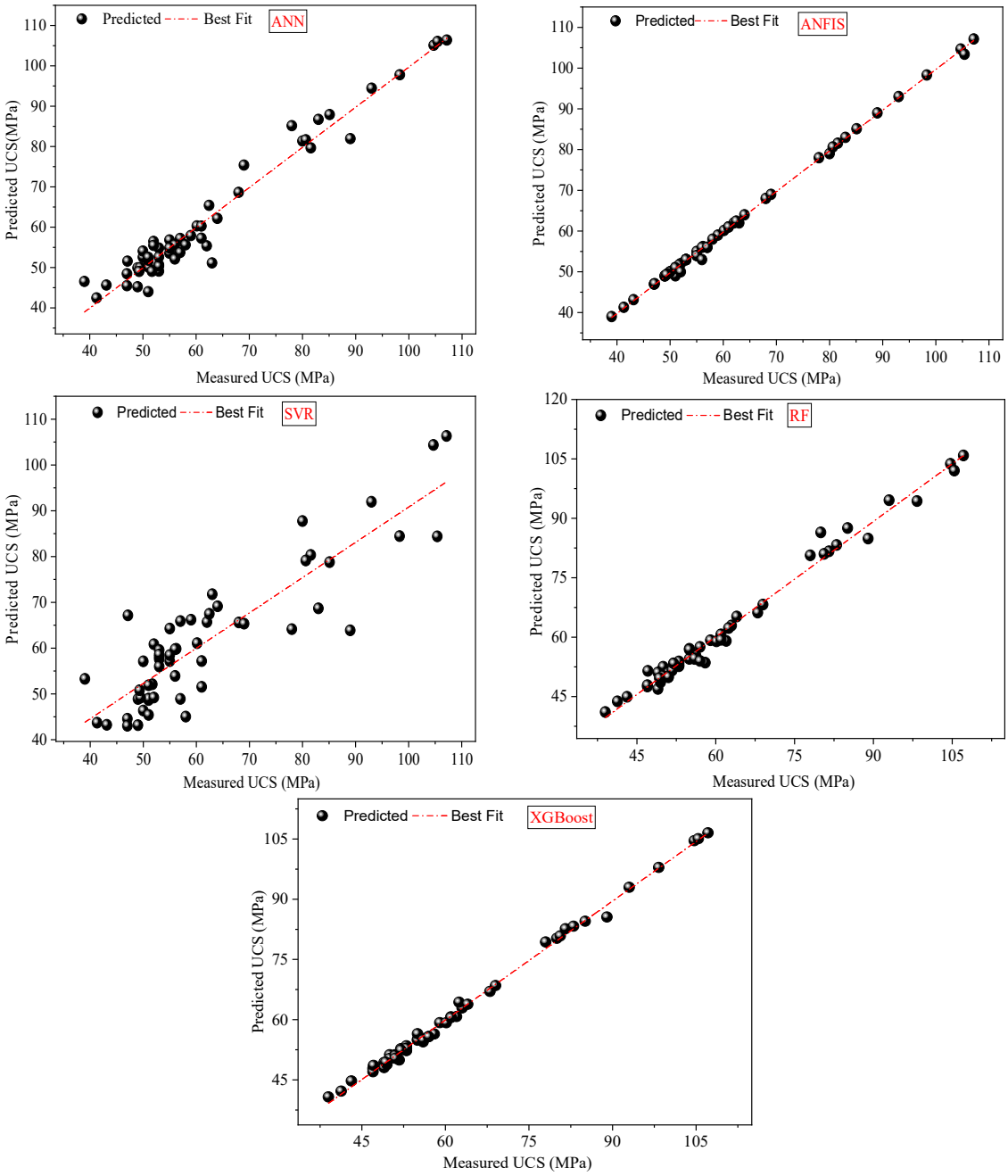

Figure 9. Scatter plot of measured and predicted values of models on the training dataset.

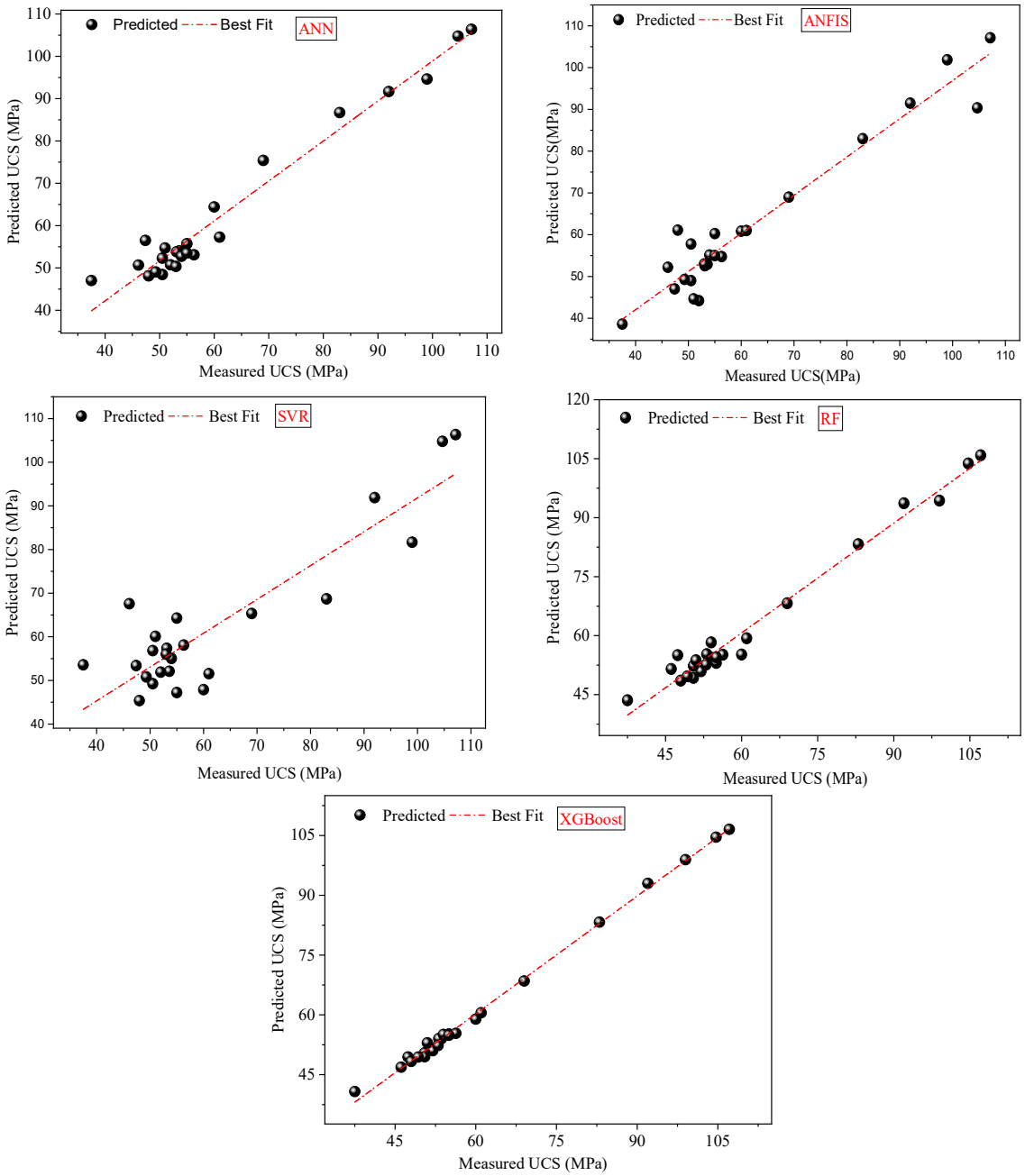

Figure 10. Test dataset scatter plot of measured and predicted values.

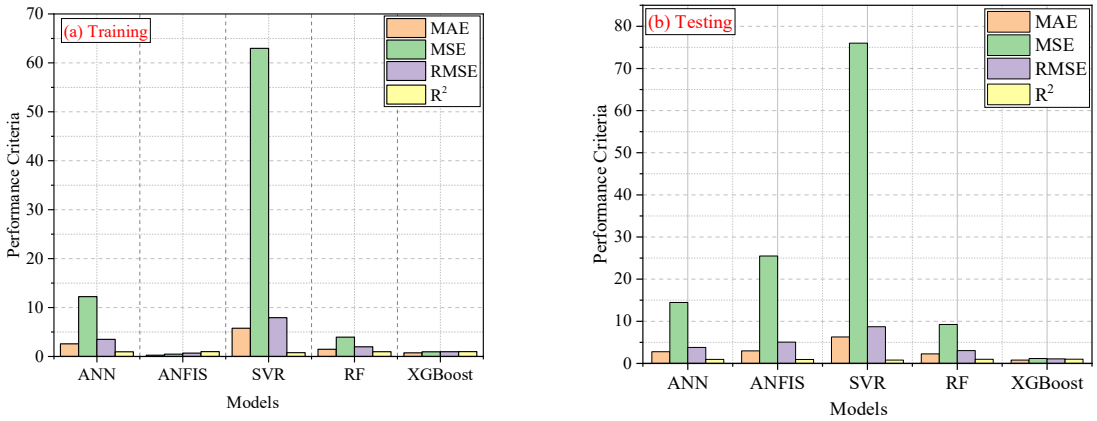

Figure 11 a) Prediction performance of training data b) Prediction performance of testing data

For further comparison and analysis of the developed models, multiple evaluation criteria were considered through a combination of Taylor diagrams shown in Figure 12. Taylor diagrams deliver a more instinctual valuation of the performance between models than a single model evaluation index. In recent years, the Taylor diagram has become an effective method for evaluating and inspecting models by displaying relevant information from multiple models [51]. As can be seen from the Taylor diagram, the XGBoost model predicts the best results for UCS among all the developed models. More precisely, due to its high-performance accuracy, the XGBoost model is recommended as a more significant model for UCS (MPa) prediction. The models' accuracy is placed in the following order; XGBoost > RF > ANN > ANFIS > SVR. Besides, the K-fold cross-validation (K = 5 ~10) was employed to confirm the stability and generality of each model. The XGBoost model had a R^2 over 0.98 across folds, with negligible variation in RMSE, indicating robust reliability across various data partitions. RF demonstrated uniform performance across folds, signifying robustness. Conversely, the SVR model exhibited greater variance in its performance indicators, highlighting its susceptibility to the amount and distribution of training data. Ensemble models facilitate the assessment of feature relevance, offering insights into the relative contributions of each input parameter. Both RF and XGBoost analyses indicated that the $Is_{(50)}$ and R_n are the most significant predictors of UCS, but η and AIV exhibit an inverse relationship with UCS. The predictive accuracy achieved in this study surpasses the performance reported in earlier UCS modeling efforts. Table 4 presents a comparison between the results of the present study and those reported in previous research. The observed improvement highlights the effectiveness of gradient boosting algorithms in rock mechanics, especially for modeling complex and variable geological data with limited sample sizes.

Table 4. Comparison between previous studies with the current study.

Models	Output	Performance(R^2)	References
ANFIS	UCS	0.98	[21]
ICA-ANN	UCS	0.94	[22]
BAS-RF	UCS	0.97	[25]
ANN	UCS	0.92	[40]
ANN	UCS	0.92	[32]
XGBoost-FA	UCS	0.98	[35]
SVR, XGBoost	UCS	0.93	[24]
ANFIS	UCS	0.95	[36]
XGBoost, RF	UCS	0.99,0.97	**This study**

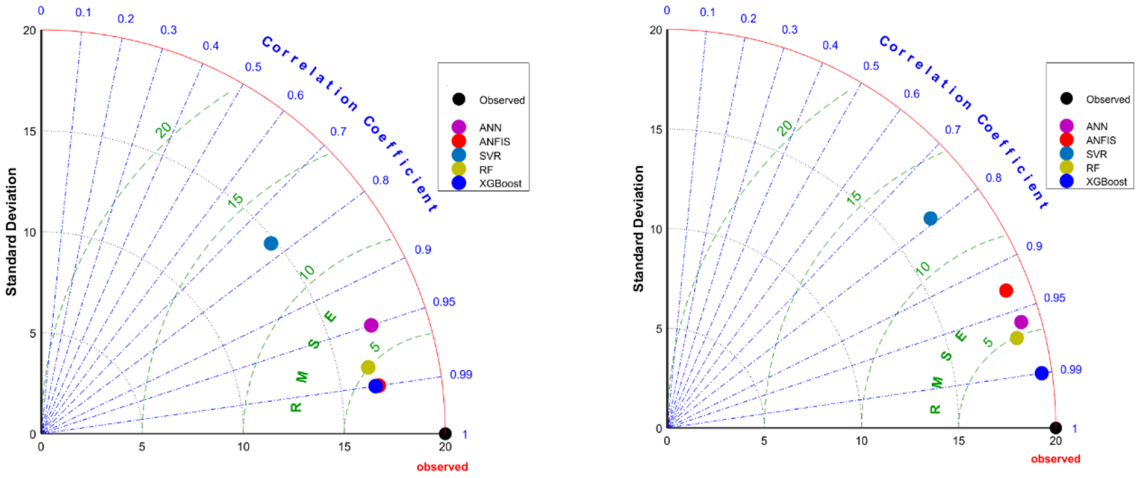

Figure 12. Taylor diagrams of different models for UCS prediction (a) training (b) testing.

8. Conclusions

This study developed five ML models including ANN, ANFIS, SVR, RF and XGBoost to predict the UCS (MPa) of sandstone in the Murree and Kamlial formation in the Muzaffarabad area, northwestern Himalayas in Pakistan. The input parameters such as η, $Is_{(50)}$, Rn and AIV were used. The MAE, MSE, RMSE and R^2 were used as performance indicators to evaluate the model's performance. The performance of models was evaluated by means of the testing dataset.

The values of the performance indicators—MAE, MSE, RMSE, and R^2—were 2.77, 14.46, 3.803, and 0.96 for the ANN model, and 2.968, 25.49, 5.049, and 0.93 for the ANFIS model, respectively. The SVM model with a linear kernel function yielded the highest MAE (6.29), MSE (76.01), RMSE (8.718), and the lowest R^2 (0.79). In testing, the MAE, MSE, RMSE, and R^2 values for the RF model were 2.266, 9.238, 3.033, and 0.97, respectively. The corresponding values for the XGBoost model were 0.789, 1.167, 1.080, and 0.99.

Therefore, based on the performance criteria, the XGBoost model is considered the best model for predicting UCS (MPa) and is recommended for predicting UCS (MPa) of sandstones and similar rocks and overcoming the problems of sample collection, cost, and transportation in the study area.

This study was conducted on a single rock type (Sandstone) and could be further examined for other rocks such as limestone, granite, marble, etc. Furthermore, the study will be extended by considering other boosting models such as LightGBM, CatBoost, and AdaBoost compared to the current recommended model. The application of different optimisation models will be used to boost the accuracy of the proposed model.

References

[1]. Barzegar, R., Sattarpour, M., Nikudel, M. R., & Moghaddam, A. A. (2016). Comparative evaluation of artificial intelligence models for prediction of uniaxial compressive strength of travertine rocks, case study: Azarshahr area, NW Iran. *Modeling Earth Systems and Environment*, *2*(2), 76.

[2]. Beiki, M., Majdi, A., & Givshad, A. D. (2013). Application of genetic programming to predict the uniaxial compressive strength and elastic modulus of carbonate rocks. *International Journal of Rock Mechanics and Mining Sciences*, *63*, 159-169.

[3]. Ceryan, N., Okkan, U., & Kesimal, A. (2012). Application of generalized regression neural networks in predicting the unconfined compressive strength of carbonate rocks. *Rock mechanics and rock engineering*, *45*(6), 1055-1072.

[4]. Sharma, L. K., Vishal, V., & Singh, T. N. (2017). Developing novel models using neural networks and fuzzy systems for the prediction of strength of rocks from key geomechanical properties. *Measurement*, *102*, 158-169.

[5]. Jalali, S. H., Heidari, M., & Mohseni, H. (2017). Comparison of models for estimating uniaxial compressive strength of some sedimentary rocks from Qom Formation. *Environmental Earth Sciences*, *76*(22), 753.

[6]. Cevik, A., Sezer, E. A., Cabalar, A. F., & Gokceoglu, C. (2011). Modeling of the uniaxial compressive strength of some clay-bearing rocks using neural network. *Applied Soft Computing*, *11*(2), 2587-2594.

[7]. Yesiloglu-Gultekin, N. U. R. G. Ü. L., Gokceoglu, C., & Sezer, E. A. (2013). Prediction of uniaxial compressive strength of granitic rocks by various nonlinear tools and comparison of their performances. *International Journal of Rock Mechanics and Mining Sciences*, *62*, 113-122.

[8]. Cao, J., Gao, J., Nikafshan Rad, H., Mohammed, A. S., Hasanipanah, M., & Zhou, J. (2022). A novel systematic and evolved approach based on XGBoost-firefly algorithm to predict Young's modulus and unconfined compressive strength of rock. *Engineering with computers*, *38*(Suppl 5), 3829-3845.

[9]. Singh, R., Vishal, V., Singh, T. N., & Ranjith, P. G. (2013). A comparative study of generalized regression neural network approach and adaptive neuro-fuzzy inference systems for prediction of unconfined compressive strength of rocks. *Neural Computing and Applications*, *23*(2), 499-506.

[10]. Suthar, M. (2020). Applying several machine learning approaches for prediction of unconfined compressive strength of stabilized pond ashes. *Neural Computing and Applications*, *32*(13), 9019-9028.

[11]. Torabi, S. R., Ataei, M., & Javanshir, M. (2011). Application of Schmidt rebound number for estimating rock strength under specific geological conditions. *Journal of Mining and Environment*.

[12]. Moshrefi, S., Shahriar, K., Ramezanzadeh, A., & Goshtasbi, K. (2018). *Prediction of ultimate strength of shale using artificial neural network. J Min Environ 9 (1): 91–105*.

[13]. Fang, Q., Yazdani Bejarbaneh, B., Vatandoust, M., Jahed Armaghani, D., Ramesh Murlidhar, B., & Tonnizam Mohamad, E. (2021). Strength evaluation of granite block samples with different predictive models. *Engineering with computers*, *37*(2), 891-908.

[14]. Jahed Armaghani, D., Safari, V., Fahimifar, A., Mohd Amin, M. F., Monjezi, M., & Mohammadi, M. A. (2018). Uniaxial compressive strength prediction through a new technique based on gene expression programming. *Neural Computing and Applications*, *30*(11), 3523-3532.

[15]. Singh, V. K., Singh, D., & Singh, T. N. (2001). Prediction of strength properties of some schistose rocks from petrographic properties using artificial neural networks. *International Journal of Rock Mechanics and Mining Sciences*, *38*(2), 269-284.

[16]. Fattahi, H., & Babanouri, N. (2017). Predicting tensile strength of rocks from physical properties based on support vector regression optimized by cultural algorithm. *Journal of Mining and Environment*, *8*(3), 467-474.

[17]. Jalali, S. H., Heidari, M., & Mohseni, H. (2017). Comparison of models for estimating uniaxial compressive strength of some sedimentary rocks from Qom Formation. *Environmental Earth Sciences*, *76*(22), 753.

[18]. Abdi, Y., Garavand, A. T., & Sahamieh, R. Z. (2018). Prediction of strength parameters of sedimentary rocks using artificial neural networks and regression analysis. *Arabian Journal of Geosciences*, *11*(19), 587.

[19]. Fattahi, H. (2020). A new method for forecasting uniaxial compressive strength of weak rocks. *Journal of Mining and Environment*, *11*(2), 505-515.

[20]. Shahani, N. M., Zheng, X., Liu, C., Hassan, F. U., & Li, P. (2021). Developing an XGBoost regression model for predicting young's modulus of intact sedimentary rocks for the stability of surface and subsurface structures. *Frontiers in Earth Science*, *9*, 761990.

[21]. Jahed Armaghani, D., Tonnizam Mohamad, E., Momeni, E., Narayanasamy, M. S., & Mohd Amin, M. F. (2015). An adaptive neuro-fuzzy inference system for predicting unconfined compressive strength and Young's modulus: a study on Main Range granite. *Bulletin of engineering geology and the environment*, *74*(4), 1301-1319.

[22]. Armaghani, D. J., Amin, M. F. M., Yagiz, S., Faradonbeh, R. S., & Abdullah, R. A. (2016). Prediction of the uniaxial compressive strength of sandstone using various modeling techniques. *International Journal of Rock Mechanics and Mining Sciences*, *85*, 174-186.

[23]. Zorlu, K., Gokceoglu, C., Ocakoglu, F., Nefeslioglu, H. A., & Acikalin, S. J. E. G. (2008). Prediction of uniaxial compressive strength of sandstones using petrography-based models. *Engineering Geology*, *96*(3-4), 141-158.

[24]. Wan, Z., Xu, Y., & Šavija, B. (2021). On the use of machine learning models for prediction of compressive strength of concrete: influence of dimensionality reduction on the model performance. *Materials*, *14*(4), 713.

[25]. Zhang, J., Ma, G., Huang, Y., Aslani, F., & Nener, B. (2019). Modelling uniaxial compressive strength of lightweight self-compacting concrete using random forest regression. *Construction and Building Materials*, *210*, 713-719.

[26]. Mai, H. V. T., Nguyen, T. A., Ly, H. B., & Tran, V. Q. (2021). Prediction compressive strength of concrete containing GGBFS using random forest model. *Advances in Civil Engineering*, *2021*(1), 6671448.

[27]. Matin, S. S., Farahzadi, L., Makaremi, S., Chelgani, S. C., & Sattari, G. H. (2018). Variable selection and prediction of uniaxial compressive strength and modulus of elasticity by random forest. *Applied Soft Computing*, *70*, 980-987.

[28]. Nguyen-Sy, T., Wakim, J., To, Q. D., Vu, M. N., Nguyen, T. D., & Nguyen, T. T. (2020). Predicting the compressive strength of concrete from its compositions and age using the extreme gradient boosting method. *Construction and Building Materials*, *260*, 119757.

[29]. Negara, A., Ali, S., AlDhamen, A., Kesserwan, H., & Jin, G. (2017, April). Unconfined compressive strength prediction from petrophysical properties and elemental spectroscopy using support-vector regression. In *SPE Kingdom of Saudi Arabia Annual Technical Symposium and Exhibition* (p. D043S036R002). SPE.

[30]. Sun, J., Zhang, J., Gu, Y., Huang, Y., Sun, Y., & Ma, G. (2019). Prediction of permeability and unconfined compressive strength of pervious concrete using evolved support vector regression. *Construction and Building Materials*, *207*, 440-449.

[31]. Wang, M., Wan, W., & Zhao, Y. (2020). Prediction of the uniaxial compressive strength of rocks from simple index tests using a random forest predictive model. *Comptes Rendus. Mécanique*, *348*(1), 3-32.

[32]. Abdi, Y., Yusefi-Yegane, B., & Jamshidi, A. (2021). Estimation of mechanical properties of sandstones from petrographic characteristics using artificial neural networks (ANNs).

[33]. Koken, E. (2024). Estimating uniaxial compressive strength of pyroclastic rocks using soft computing techniques. *Journal of Mining and Environment*, *15*(3), 977-990.

[34]. Jamshidi, A. (2022). A comparative study of point load index test procedures in predicting the uniaxial compressive strength of sandstones. *Rock Mechanics and Rock Engineering*, *55*(7), 4507-4516.

[35]. Cao, J., Gao, J., Nikafshan Rad, H., Mohammed, A. S., Hasanipanah, M., & Zhou, J. (2022). A novel systematic and evolved approach based on XGBoost-firefly algorithm to predict Young's modulus and unconfined compressive strength of rock. *Engineering with computers*, *38*(Suppl 5), 3829-3845.

[36]. Shahani, N. M., Zheng, X., Liu, C., Li, P., & Hassan, F. U. (2022). Application of soft computing methods to estimate uniaxial compressive strength and elastic modulus of soft sedimentary rocks. *Arabian Journal of Geosciences*, *15*(5), 384.

[37]. Heidari, M., Mohseni, H., & Jalali, S. H. (2018). Prediction of uniaxial compressive strength of some sedimentary rocks by fuzzy and regression models. *Geotechnical and Geological Engineering*, *36*(1), 401-412.

[38]. Jahed Armaghani, D., Tonnizam Mohamad, E., Hajihassani, M., Yagiz, S., & Motaghedi, H. (2016). Application of several non-linear prediction tools for estimating uniaxial compressive strength of granitic rocks and comparison of their performances. *Engineering with Computers*, *32*(2), 189-206.

[39]. Asadizadeh, M. (2020). Predicting unconfined compressive strength of intact rock using new hybrid intelligent models.

[40]. Kamani, M., Khaleghi Esfahani, M., & Ajalloeian, R. (2020). Prediction of carbonate aggregates properties through physical tests. *Geotechnical and Geological Engineering*, *38*(2), 2169-2186.

[41]. Mustafa, S., Khan, M. A., Khan, M. R., Sousa, L. M., Hameed, F., Mughal, M. S., & Niaz, A. (2016). Building stone evaluation—A case study of the sub-Himalayas, Muzaffarabad region, Azad Kashmir, Pakistan. *Engineering Geology*, *209*, 56-69.

[42]. ASTM. (1985). Standard Test Method for Determination of the Point Load Strength Index of Rock 1. 22(2), 1–9.

[43]. Khademi, F., Jamal, S. M., Deshpande, N., & Londhe, S. (2016). Predicting strength of recycled aggregate concrete using artificial neural network, adaptive neuro-fuzzy inference system and multiple linear regression. *International journal of sustainable built environment*, *5*(2), 355-369.

[44]. Tariq, Z., Abdulraheem, A., Mahmoud, M., Elkatatny, S., Ali, A. Z., Al-Shehri, D., & Belayneh, M. W. (2019). A new look into the prediction of static Young's modulus and unconfined compressive strength of carbonate using artificial intelligence tools. *Petroleum Geoscience*, *25*(4), 389-399.

[45]. Sezer, E. A., Nefeslioglu, H. A., & Gokceoglu, C. (2014). An assessment on producing synthetic samples by fuzzy C-means for limited number of data in prediction models. *Applied Soft Computing*, *24*, 126-134.

[46]. Teymen, A., & Mengüç, E. C. (2020). Comparative evaluation of different statistical tools for the prediction of uniaxial compressive strength of rocks. *International Journal of Mining Science and Technology*, *30*(6), 785-797.

[47]. Farid, M., HosseinAbadi, M. M., Yazdani-Chamzini, A., Yakhchali, S. H., & Basiri, M. H. (2013). Developing a new model based on neuro-fuzzy system for predicting roof fall in coal mines. *Neural computing and applications*, *23*(Suppl 1), 129-137.

[48]. Longjun, D., Xibing, L., Ming, X., & Qiyue, L. (2011). Comparisons of random forest and support vector machine for predicting blasting vibration characteristic parameters. *Procedia Engineering*, *26*, 1772-1781.

[49]. Janitza, S., Tutz, G., & Boulesteix, A. L. (2016). Random forest for ordinal responses: prediction and variable selection. *Computational Statistics & Data Analysis*, *96*, 57-73.

[50]. Friedman, J. H. (2001). Greedy function approximation: a gradient boosting machine. *Annals of statistics*, 1189-1232.

[51]. Qiu, Y., Zhou, J., Khandelwal, M., Yang, H., Yang, P., & Li, C. (2022). Performance evaluation of hybrid WOA-XGBoost, GWO-XGBoost and BO-XGBoost models to predict blast-induced ground vibration. *Engineering with Computers*, *38*(Suppl 5), 4145-4162.

[52]. Schober, P., Boer, C., & Schwarte, L. A. (2018). Correlation coefficients: appropriate use and interpretation. *Anesthesia & analgesia*, *126*(5), 1763-1768.

[53]. Ngo, H. T. T., Pham, T. A., Vu, H. L. T., & Giap, L. V. (2021). Application of artificial intelligence to determined unconfined compressive strength of cement-stabilized soil in Vietnam. *Applied Sciences*, *11*(4), 1949.

[54]. Rodriguez, J. D., Perez, A., & Lozano, J. A. (2009). Sensitivity analysis of k-fold cross validation in prediction error estimation. *IEEE transactions on pattern analysis and machine intelligence*, *32*(3), 569-575.

[55]. Huang, Y., Zhang, J., Ann, F. T., & Ma, G. (2020). Intelligent mixture design of steel fibre reinforced concrete using a support vector regression and firefly algorithm based multi-objective optimization model. *Construction and Building Materials*, *260*, 120457.

انجمن مهندسی معدن ایران
نشریه مهندسی معدن و محیط زیست
نشانی نشریه: www.jme.shahroodut.ac.ir
دانشگاه صنعتی شاهرود

کاربردهای مدل‌های یادگیری ماشین برای پیش‌بینی مقاومت فشاری تک‌محوری ماسه‌سنگ از مظفرآباد – مطالعه موردی

برکت الله[۲،۱*] و راجا خرم محمود خان[۳]

۱ .مرکز تحقیقات مهندسی ژئوتکنیک ساحلی و شهری، دانشگاه ژجیانگ، زیجینگانگ، هانگژو ۳۱۰۰۵۸، چین
۲ .مرکز محاسبات مهندسی ژئوتکنیک، دانشگاه ژجیانگ، هانگژو، ژجیانگ ۳۱۰۰۵۸، چین
۳. گروه مهندسی عمران، ساخت و ساز، معماری و محیط زیست، دانشگاه لاکیلا، لاکیلا ۶۷۱۰۰، ایتالیا

اطلاعات مقاله

تاریخ ارسال: ۲۰۲۵/۰۷/۰۲
تاریخ داوری: ۲۰۲۵/۱۱/۰۸
تاریخ پذیرش: ۲۰۲۵/۱۲/۲۹

DOI:10.22044/jme.2025.16419.3206

کلمات کلیدی

اعتبارسنجی متقابل K-تایی
یادگیری ماشین
ماسه سنگ
مقاومت فشار تک محوره (UCS)
XGBoost

چکیده

مقاومت فشاری تک‌محوری (UCS) یک ویژگی ضروری برای توصیف و طبقه‌بندی توده‌های سنگ است و جزء مهمی از معیارهای شکست سنگ را با کاربردهای گسترده در مهندسی معدن و ژئوتکنیک تشکیل می‌دهد. هدف این مطالعه ارزیابی عملکرد مدل‌های مختلف یادگیری ماشین (ML) در پیش‌بینی مقاومت فشاری تک‌محوری ماسه‌سنگ به‌دست‌آمده از سازندهای موری و کاملیال در منطقه مظفرآباد، شمال غربی هیمالیا، پاکستان است. مدل‌های ML - یعنی شبکه عصبی مصنوعی (ANN)، سیستم استنتاج فازی-عصبی تطبیقی (ANFIS)، رگرسیون بردار پشتیبان (SVR)، جنگل تصادفی (RF) و تقویت گرادیان شدید (XGBoost) - برای پیش‌بینی مقاومت فشاری تک‌محوری (MPa) بر اساس تخلخل (η)، شاخص بار نقطه‌ای (Is(50))، مقدار بازگشت چکش اشمیت (Rn) و مقدار ضربه سنگدانه (AIV) به عنوان متغیرهای ورودی توسعه داده شدند. یک مجموعه داده حاوی ۸۰ نقطه با استفاده از نسبت تقسیم ۷۰:۳۰ برای مجموعه‌های آموزش و آزمایش تقسیم‌بندی شد. اعتبارسنجی متقابل K-fold (با ۵ تا ۱۰ fold) برای افزایش قابلیت تعمیم مدل‌ها به کار گرفته شد. عملکرد مدل‌ها با استفاده از میانگین خطای مطلق (MAE)، میانگین مربعات خطا (MSE)، جذر میانگین مربعات خطا (RMSE) و ضریب تعیین (R^2) ارزیابی شد. نتایج نشان داد که مدل XGBoost با دستیابی به مقدار R^2 بالا برابر با ۰.۹۹ و مقادیر خطای پایین برای (0.789) MAE، (1.168) MSE و RMSE (1.080)) از سایر مدل‌ها بهتر عمل کرد. دقت کلی مدل‌ها را می‌توان به شرح زیر رتبه‌بندی کرد: XGBoost > RF > ANN > ANFIS > SVR. این مطالعه معیاری برای پیش‌بینی UCS ماسه‌سنگ‌ها و سنگ‌های مشابه ارائه می‌دهد که در آن‌ها زمین‌شناسی پیچیده، جمع‌آوری نمونه‌های دست‌نخورده را پیچیده می‌کند..

نویسنده مسئول مکاتبات: barkat_ullah12@outlook.com (ب. الله)